Star-to-bottlebrush transition in extensional and shear deformation of unentangled polymer melts

Aristotelis Zografos,[†] Helena A. All,[‡] Alice B. Chang,[†] Marc A. Hillmyer,[*,‡] Frank S. Bates[*,†]

[†]Department of Chemical Engineering and Materials Science, University of Minnesota, Minneapolis, MN, 55455-0132

[‡] Department of Chemistry, University of Minnesota, Minneapolis, MN, 55455-0431

*Corresponding authors (e-mail addresses: bates001@umn.edu; hillmyer@umn.edu)

TOC Graphic

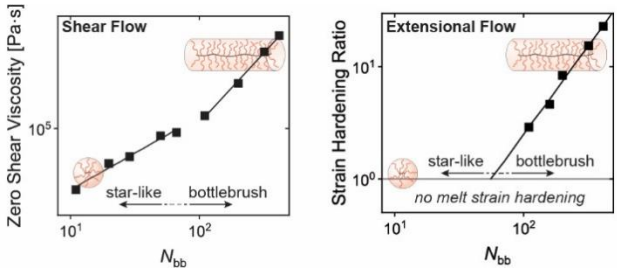

Abstract

A series of model poly((±)-lactide) (PLA) graft copolymers was synthesized by ring-opening metathesis polymerization and used to probe the star-to-bottlebrush transition in shear and extensional flows. Ten samples with backbone degrees of polymerization $11 \leq N_{bb} \leq 420$ were investigated using small-amplitude oscillatory shear (SAOS) and extensional rheometry measurements. Each contained one PLA side chain of length $N_{sc} = 72$ per two backbone repeating units on average (graft density of $z = 0.5$). The star-like to bottlebrush transition was identified at $N_{bb} = 50–69$ using SAOS. In extension, melt strain hardening is absent in the star-like melts ($N_{bb} \leq 50$) but is prominent in the bottlebrush limit ($N_{bb} > 69$). The onset of melt strain hardening occurs at a timescale equivalent to the Rouse time of the backbone. A molecular interpretation of these results builds upon recent conjectures related to strain-induced increases in interchain friction in bottlebrush polymers. These findings will be useful in designing bottlebrush melts that strain

harden, which is critical in various types of processing methods involving extensional flows, including foaming, 3D printing, and film-blowing.

Introduction

The usefulness of a commodity plastic is constrained by the number of ways it can be shaped, molded, or formed into products. As society moves towards biobased plastics capable of tailored degradation, these limitations must be considered.[1] Polylactide (PLA), currently the most widely produced biobased and industrially-compostable plastic, offers an illustrative case.[2] . PLA has a low extensional viscosity, which makes it more susceptible to fracture during extensional melt deformation.[3,4,5] As a 'weak melt', PLA is less amenable to extension-dominated melt processing methods such as film-blowing, foaming, and thermoforming,[6] thus limiting its application range. A common industrial solution is to incorporate long chain branching (LCB) into the architecture of PLA, which is often accomplished using a chain-extending reactive additive. Additives such as BASF Joncryl® are linear polymers decorated with functional groups along the chain that can react with the end-groups of PLA, thus forming LCB through a *grafting-to* process.[7,8,9] Importantly, LCB enables melt-strain hardening (MSH) upon extensional deformation, which increases the extensional viscosity, thus making the melt stronger.[10] MSH limits fracture by stabilizing mechanical instabilities such as necking and narrows the dimensional tolerance of the processed part.[11,12,13,14] It is advantageous to melt processing and, in the case of PLA, offers a tool that can be used to improve the melt processability and increase its application space.

LCB specifically refers to branches that are above the critical molar mass (M_c) thus forming mechanically effective entanglements, where M_c is approximately 2–3 times larger than the entanglement molar mass (M_e).[10] LCB induces MSH by pinning segments of a polymer between two branch points, thereby restricting stress relaxation to a slow process referred to as 'arm retraction'.[10,15] As a result, non-linear viscoelastic flow such as MSH becomes more pronounced and accessible at slower deformation rates.[10,15] As these pinned segments are shortened and approach the monomeric limit, MSH should become negligible. Recent reports suggest bottlebrush polymers can exhibit substantial MSH, even under circumstances where no pinned segments

exist,[16,17,18] suggesting a distinct molecular relaxation mechanism. Note, the label "bottlebrush" implies that the side chains (i.e., branches or grafts) are packed closely enough to sterically force the polymer backbone into an extended conformation. A "comb" polymer refers to the limit where the branches are spaced sparsely and do not interact. Several theoretical [19,20,21,22] and experimental[16,22,23] reports have identified additional gradations e.g., 'loose comb' and 'dense brush'.

Haugan et al. showed that a sudden change in M_e occurs at the comb-to-bottlebrush transition as the graft density (z) is changed.[23] In terms of extensional melt flow, Abbasi and coworkers recently attempted to distinguish between comb and bottlebrush polymers by probing how z influences the MSH for a series of narrowly disperse polystyrene-based samples with equal backbone (N_{bb}) and side chain (N_{sc}) degrees of polymerization.[16,24] A non-monotonic trend was observed where the MSH increased as more grafts were added to the backbone and then decreased when z became too high; the sudden decrease in MSH was associated with a comb-to-bottlebrush transition. No molecular interpretation has been proposed to support why the bottlebrush polymers were capable of MSH, and to date no molecular model that accurately predicts this behavior has been advanced.[25,26,27] Recently, López-Barrón and coworkers investigated the extensional melt-flow properties of poly(α-olefin) bottlebrushes, where each side chain was separated by 2 carbon atoms.[17,18] They observed substantial MSH behavior and attributed this to an increase in side chain interdigitation as the polymers aligned in the flow direction. This was postulated to increase intermolecular friction, leading to enhanced extensional viscosity and MSH. However, there is limited experimental evidence to support this mechanism.

None of the previous studies of bottlebrush polymers probed the influence of N_{bb} on MSH during uniaxial extension. We expect this to be an important parameter because of its influence on linear viscoelastic shear flow,[28,29] thermodynamic phase behavior,[30] and chain conformation[31] due to what has been attributed to a star-to-bottlebrush transition. When N_{bb} is sufficiently smaller than N_{sc}, the chain conformation is star-like (i.e., spherical confirmations), while at large N_{bb},

bottlebrush polymers assume more cylindrical conformations. Note, the phrase 'star-like' is used to emphasize that the branches do not originate from a single junction, as with traditional star polymers, and that the extent of this regime is a function of N_{bb} and N_{sc}. The spherical conformation of dilute star-like polymers in a good solvent was confirmed by small-angle neutron scattering (SANS).[31]

To probe the star-to-bottlebrush transition (SBT) in extensional deformation, we synthesized a library of model graft polymers with varying N_{bb} using controlled polymerization techniques. The SBT potentially coincides with a change in scaling of the zero-shear viscosity as a function of N_{bb}.[28] In this study, small-amplitude oscillatory shear (SAOS) rheometry was used to identify this transition and determine if it was correlated with changes in the uniaxial extensional flow behavior, most notably the transient, non-linear extensional viscosity (i.e., melt strain hardening). SAOS rheometry was used to correlate molecular relaxation times and entanglement phenomena to the extensional rheology data. A molecular interpretation of the experimental results that invokes aforementioned ideas related to interchain friction is proposed.[18]

Results and Discussion

Grafting-through ring-opening metathesis copolymerization was used to synthesize all polymers using methods described in the literature,[32,33] as illustrated in Figure 1A. A poly((±)-lactide) ω-norbornenyl macromonomer (MM) was copolymerized with a dimethyl-ester norbornene (DME) comonomer yielding graft polymers with a poly(norbornene) backbone and poly((±)-lactide) side chains (Figure 1A). DME was used to access larger values of N_{bb} without the addition of more grafts, which was done to limit the total molar mass of each polymer. For all copolymerizations, an equimolar initial feed composition (f_0) was used to target $z = f_{0,MM} = 0.5$, which corresponds to one graft for every two backbone repeat units. Apart from one sample where $N_{sc} = 25$, all graft polymers had $N_{sc} = 72$. We recently found that N_{sc} and f_0 can impact the graft distribution along the backbone (i.e., gradient, random).[34] For each polymer, the conditions used here result in a near-random distribution of grafts. The SBT was probed by varying N_{bb} between

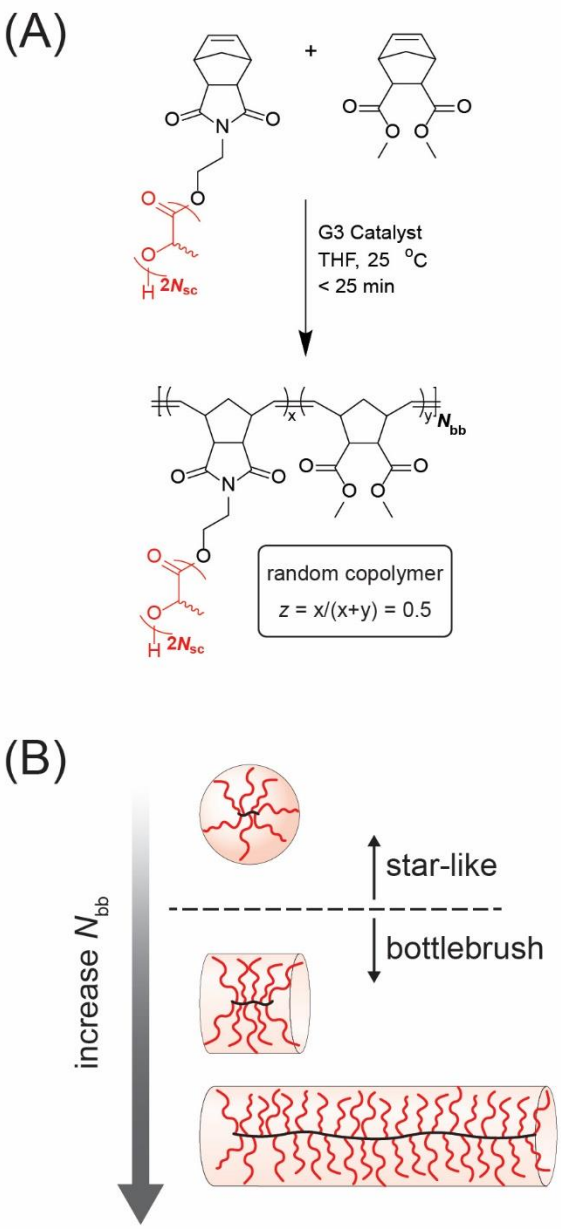

Figure 1. (A) Graft-through ring opening metathesis reaction scheme used to synthesize the polymers studied in this work. A previous report demonstrates that these copolymerizations produce random copolymers.[34] All copolymers have a graft density of $z = 0.5$, corresponding to one graft per two backbone repeat units on average. All rheological data, apart from that shown in Figure 14, was acquired from polymers with $N_{sc} = 72$. (B) Schematic illustration of the star-to-bottlebrush transition with increasing N_{bb}.

11 and 420 (Figure 1B). Size exclusion chromatography (SEC) traces demonstrate the control over molar mass and low dispersity values typically associated with ROMP of norbornene derivatives

(Figure 2). Apart from the largest polymer, the molar mass distribution of each sample was relatively narrow ($Đ < 1.1$). The slight increase in dispersity for $N_{bb} = 420$ ($Đ = 1.18$) is consistent with findings from Radzinski et al. for a similar polymerization, which demonstrated the reaction to become less controlled at decreased catalyst loadings.[35] Specific details regarding molecular characterization can be found in Table 1 and Reference 34.[34]

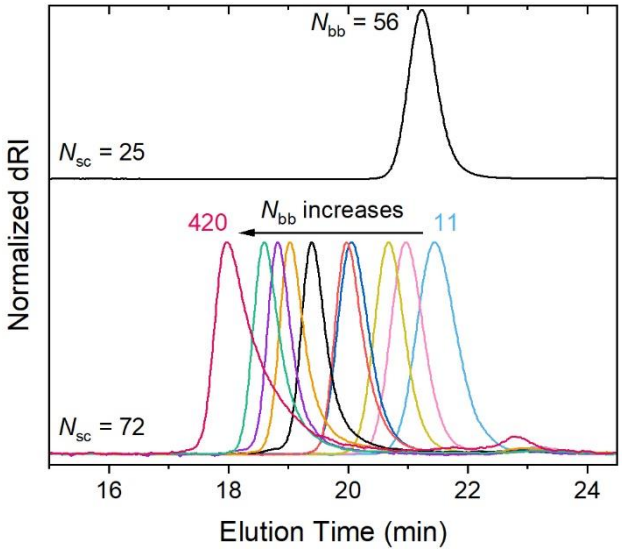

Figure 2. Normalized size exclusion chromatography (SEC) data collected using a differential refractometer with tetrahydrofuran as the eluent. Traces correspond to graft polymers with different backbone and side-chain degrees of polymerization (N_{bb} and N_{sc}, respectively). All samples maintained a constant grafting density ($z = 0.5$), which corresponds to an average of one graft per two backbone repeat units. Values and methods for determining N_{bb},N_{sc}, and z for each polymer can be found in Table 1.

Differential scanning calorimetry (DSC, Figure S1) traces show no melting endotherms, indicating that the materials are fully amorphous, consistent with the atactic microstructure of the poly(±-lactide) side chains. Only one glass transition (T_g) was identified, which correlates well with that of linear PLA. This is expected, given the low backbone composition (PLA > 95 wt%) of each graft polymer. For polymers with $N_{sc} = 72$, the T_g values showed no statistically significant dependence on N_{bb} ($\overline{T}_g \pm \sigma = 51.9 \pm 1.9$ °C), which is consistent with literature

observations.[29, 36, 37, 38] Small-angle x-ray scattering (SAXS) traces exhibited no evidence of microphase separation (Figure S2).

Table 1. Molecular characterization of each graft copolymer.

N_{bb}[a]	z[c]	$M_{w,\ total}$ [kg mol^{-1}][d]	$Đ$[d]
		N_{sc} = 72[b]	
11	0.50	58	1.06
20	0.50	109	1.03
29	0.52	162	1.02
50	0.49	266	1.01
67	0.52	378	1.01
110	0.47	562	1.03
160	0.49	828	1.04
200	0.50	1080	1.04
320	0.50	1740	1.04
420	0.49	2240	1.18
		N_{sc} = 25[b]	
56	0.51	115	1.01

[a]Calculated using Equation S2.

[b]Determined using ^{1}H-NMR end-group analysis of the macromonomer. Details regarding macromonomer synthesis and characterization can be found in the literature.[34] All polymers have a side chain dispersity of $Đ$ = 1.02.[34]

[c]Grafting density (z) was determined from the initial monomer feedstock composition using ^{1}H-NMR and assumes full monomer conversion using methods described in the literature.[34] Values suggest that 50% of the backbone repeat units have side chains.

[d]Determined using THF-SEC MALS, assuming a dn/dc of 0.05 mL/g, which corresponds to polylactide (PLA). Each polymer is ≥ 95 wt% PLA.

Small Amplitude Oscillatory Shear (SAOS) Rheology

Master curves of polymers with N_{sc} = 72 at a reference temperature of $T_{ref} = \overline{T}_g + 34$ °C are shown in Figure 3, which use the shift factors plotted in Figure 4. The shift factors collapse onto a single curve (Figure 4) that was fit to the Williams-Landel-Ferry equation,

$$\log(a_T) = \frac{-C_1(T - T_{ref})}{C_2 + (T - T_{ref})} \quad (1)$$

yielding the parameters $C_1 = 6.2 \pm 0.2$, and $C_2 = 71.0 \pm 1.4$ °C. The results imply that, at constant N_{sc} and z, the temperature dependence of chain relaxation is not a function of N_{bb}, which agrees with results from the literature.[29,38] When $T_{ref} = \overline{T}_g$, the WLF parameters become $C_1^g = 11.9$ and $C_2^g = 37.0$ °C (Figure S3). These values are consistent with what is typically reported for polymer melts $C_1^g = 10\text{-}15$ and $C_2^g = 40\text{-}60$ °C and with values reported by Hu et al. for similar PLA graft polymers.[38, 39]

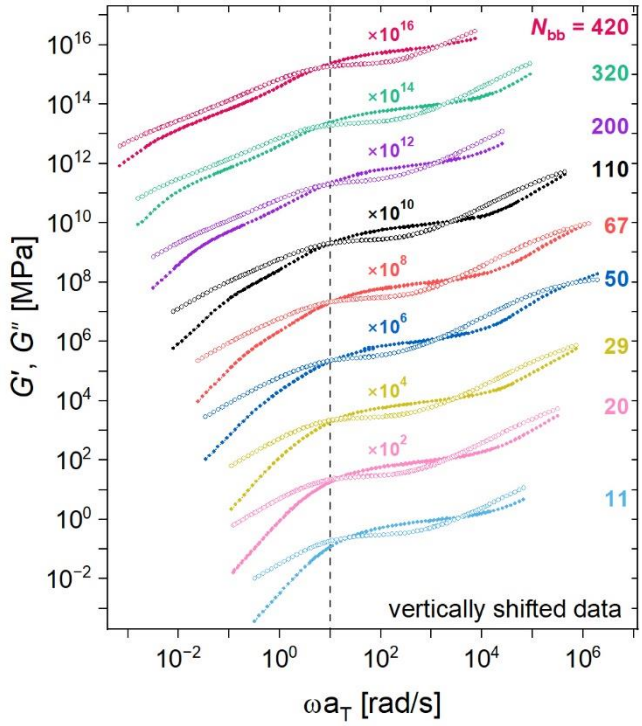

Figure 3. Master curves for samples with N_{sc} = 72 as a function of frequency using a reference temperature of $T_{ref} = \overline{T}_g + 34$ °C. Data are shifted vertically by the value indicated above each data set. Unshifted data are presented in Figure S5. Solid and open points denote G' and G'', respectively.

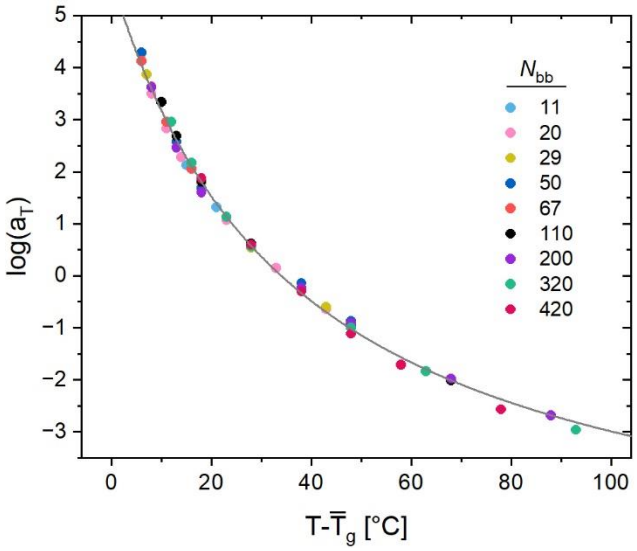

Figure 4. Shift factors for each sample with N_{sc} = 72 collected using the reference temperature of $T_{ref} = \bar{T}_g + 34$ °C. The abscissa was scaled with respect to the average glass transition temperature of all the samples. The grey curve corresponds to a global fit of all the data to the Williams-Landel-Ferry equation using the parameters $C_1 = 6.2 \pm 0.2$ and $C_2 = 71.0 \pm 1.4$ °C, which results in an *R*-squared (R^2) > 0.99. When $R^2 = 1$, the model describes all variation in the data.

The application of time-temperature-superposition (TTS) required the assumption of thermorheological simplicity. This was validated using van-Gurp Palmen (VGP) plots (Figure 5), which compare the phase angle (◦) to the magnitude of the complex modulus (|*G**|).[10,40] Both material functions are time-independent, enabling data at different temperatures to overlap without the application of a shift factor if all the relaxation modes have the same temperature dependence. In Figure 5, the data collected at different temperatures overlap well for each polymer, which supports the validity of TTS.

The dashed line in Figure 3 roughly demarcates the frequency below which differences between samples are evident. Side chain relaxations dominate the response for $\omega a_T \gtrsim 10^1$ s^{-1},

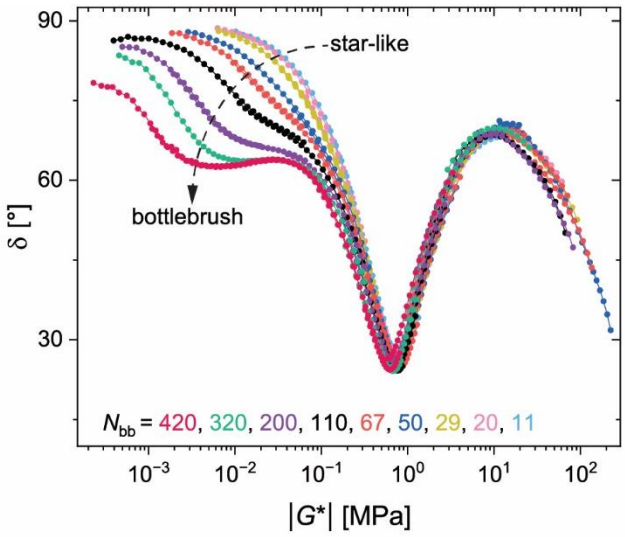

Figure 5. Van Gurp-Palmen plots for each sample with $N_{sc} = 72$. All data collapse onto a common curve above a threshold value of |G*| where side chain relaxations dominate the response. An additional minimum is evident at low |G*| as N_{bb} increases, corresponding to the star-to-bottlebrush transition.

where all samples exhibit similar behavior owing to common values of $N_{sc} = 72$. This point is clearly evidenced in the VGP plots shown in Figure 5, where all the data collapse onto a common curve above a threshold value of $|G^*|$ where side chain relaxations become predominant.[16,23,29,38,41,42] Figure S4 shows the master curve of the macromonomer, where no rubbery plateau is observed. Increasing to $N_{bb} = 11$, which corresponds to an average of six branches per molecule, results in a change in the viscoelastic behavior where a plateau-like shoulder forms, and the terminal relaxation time increases by about two orders of magnitude. Hu et al. studied PLA graft polymers with side chains of a similar molar mass and demonstrated that this shoulder region is unlikely to be associated with reptation dynamics.[38] Here, we note that the shoulder only becomes evident when multiple branches are tethered together (Figure S4). Therefore, it is attributed to relaxation of the tethered side chains, which is different than the reptation mechanism. Interestingly, this pseudo-plateau region is invariant across all values of N_{bb}, indicating it reflects single branch dynamics since $q \sim N_{bb}$, where q is the number of branches.

In Figure 3, the polymers behave differently at frequencies $\omega a_T \lesssim 10^1$. For $N_{bb} = 11$, terminal flow occurs immediately following the plateau as the frequency is reduced. For $N_{bb} = 420$, additional backbone relaxation processes occur, covering about three orders of magnitude in ωa_T, before terminal flow is achieved. This low frequency non-terminal region shrinks and eventually disappears as N_{bb} decreases. We interpret the value $N_{bb} < 67$, where the low frequency response converts to strictly terminal flow, as the transition from bottlebrush to star-like behavior.[29] This viscoelastic transition is also plainly evident in the VGP plots (Figure 5) for $|G^*| < 10^{-1}$ MPa, where a second minimum forms as N_{bb} increases. In the star-like regime ($N_{bb} < 67$), the viscoelastic response is predominantly controlled by the side chains.

Figure 6 shows the absolute value of the complex viscosity ($|\eta^*|$) of each polymer with $N_{sc} = 72$ as a function of frequency. For $N_{bb} = 420$, three distinct regions are observed in the data. At the lowest frequencies, $|\eta^*|$ approaches the zero-shear viscosity (η_0). At intermediate and high frequencies, two power law regions exist. As with the storage and loss moduli (Figures 3 and S5), all samples in the high frequency range follow a similar viscoelastic response (Figure 6, inset), attributed to the common side chain molar mass for each polymer. In the intermediate region, the viscosity is a function of N_{bb}, where the power-law scaling exponent and breadth of the region increase as N_{bb} increases. Zimm scaling is recovered at large N_{bb} (Figure 6 and S6), where $|\eta^*| \sim \omega^{-0.33}$. This was previously reported by Dalsin et al. for bottlebrush polymer melts with entangled side chains (i.e., $N_{sc} \approx 3.5N_{e,sc}$).[29] They postulated that the interior graft segments near the backbone were shielded from contributing to the viscous response, resulting in non-draining behavior. This is different from Zimm theory, which models polymers as non-draining due to the hydrodynamic interactions that exist in solution, which are not present in polymer melts.[39,43] Despite this distinction, the resulting behavior is equivalent, which gives rise to the same scaling response. In the same study, the polymers were found to be Rouse-like, $|\eta^*| \sim \omega^{-0.5}$, in the absence of side chain entanglements. Here, our data demonstrates that the grafts do not need to be well above N_e to behave as hard, non-draining spheres. Furthermore, the data shows that this behavior

is lost in the star-like limit. The intermediate scaling region disappears at $50 < N_{bb} < 67$, which further supports this value as the SBT.

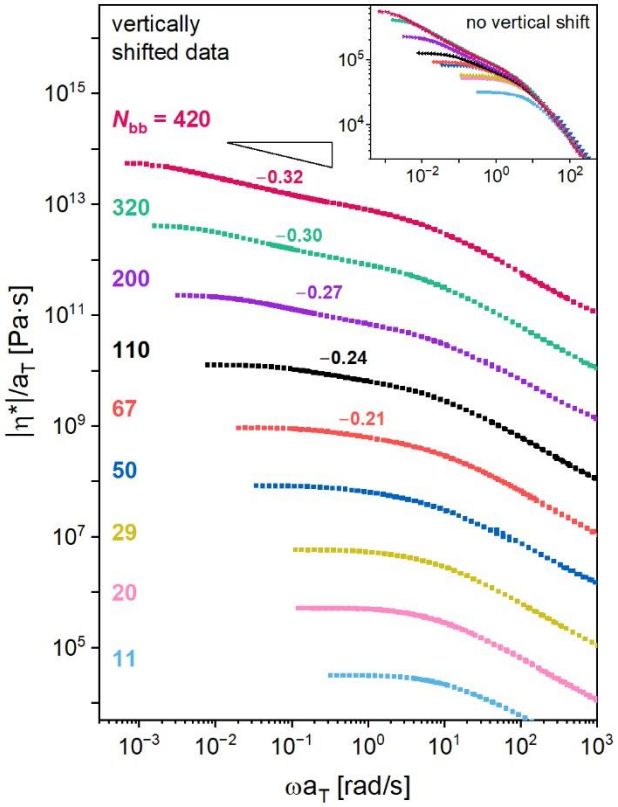

Figure 6. Absolute value of the complex viscosity as a function of frequency for samples with $N_{sc} = 72$ using a reference temperature of $T_{ref} = \overline{T}_g + 34$ °C. Data has been shifted vertically sequentially by an order of magnitude for clarity. Unshifted data can be seen in the inset.

The zero-shear viscosity (η_0) is defined as:

$$\eta_0 = \lim_{\omega \to 0} |\eta^*| . \tag{2}$$

Low frequency complex viscosity data were fit to the Carreau-Yasuda (CY) equation,

$$|\eta^*| = \eta_0 \left[1 + (\lambda\omega)^a\right]^{(n-1)/a}, \tag{3}$$

an empirical model where λ, a, and n are material constants.[10] As with other commonly used models (e.g., Cross and Carreau), the CY equation only describes a single power law region; the full relaxation spectrum of bottlebrush melts cannot be fit because two power law regions exist. For these samples, the high frequency region was not considered when determining η_0 (Figure S7).

Extrapolated results are shown in Figure 7, plotted as a function of N_{bb}. Since N_{sc} and z are constant, N_{bb} is proportional to $M_{w,total}$. A scaling transition is evident in Figure 7 at $N_{bb} \approx 70$, which

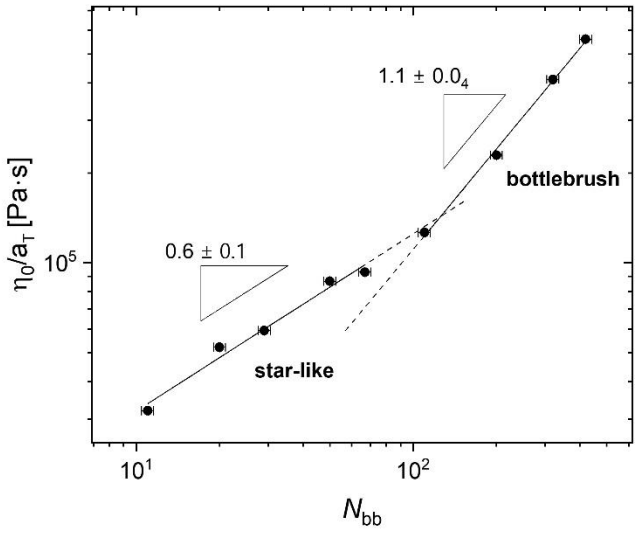

Figure 7. Zero-shear viscosity of each sample with $N_{sc} = 72$ taken at $T_{ref} = \overline{T}_g + 34$ °C. The error of the viscosity is smaller than the data points. A 5% error is assumed for the backbone degree of polymerization N_{bb}. Solid lines correspond to power law fits, where the two power law exponents are indicated. The dashed lines are extrapolated.

delineates star-like and bottlebrush melt behavior. In the Supporting Information, we provide an analysis and discussion of this two-regime model, leading to the conclusion that the onset of the SBT occurs within the range of $67 < N_{bb} < 110$, which is consistent with the transitions identified from other SAOS data (Figures 3, 5, and 6). The relatively small number of data points that define each regime challenge the ability to identify an exact value of N_{bb} that corresponds to a cross-over with statistical certainty. In the bottlebrush limit, Rouse-like behavior ($\eta_0 \sim N_{bb}$) is observed (Figure 7), indicating the absence of entanglements, since reptation scaling ($\eta_0 \sim N_{bb}^{3.4}$) is not realized.[23,39] Dalsin et al. found that Rouse scaling is lost in the star-like limit but did not characterize enough samples to quantify the behavior.[28] Here, the star-like polymers show a smaller power law exponent, $\eta_0 \sim N_{bb}^{0.6}$. As noted above, star polymers are conventionally described as having a single junction from which all arms originate. The relaxation modes of each arm are decoupled from one another; η_0 is not a function of the number of arms (q) and only

depends on N_{sc}. These conclusions are supported by numerous theoretical and experimental results.[10,44,45,46,47] What we report here is different. The zero-shear viscosity changes when N_{sc} is held constant and follows a power law dependence when the number of arms q is increased, since $q \sim N_{bb}$. We attribute this distinctly different behavior to the finite length backbone that exists for these star-like polymers, which likely contributes to the viscoelastic response.

Summarizing this section, transitions in G', G'', $|G^*|$, $|\eta^*|$, and η_0 all indicate a SBT at $50 < N_{bb} < 69$. Next, we explore whether this also impacts uniaxial extensional flow behavior.

Extensional Rheology

The melt viscosity during uniaxial flow was measured using an Extensional Viscosity Fixture (EVF), as described in the Methods section. Figure 8 shows the tensile stress growth coefficient, $\eta_E^+(t, \dot{\varepsilon}_H)$ plotted as a function of deformation time (t) for polymers with $N_{sc} = 72$. The function $\eta_E^+(t, \dot{\varepsilon}_H)$ defines the transient extensional viscosity before a steady-state value is achieved as $t \to \infty$. The steady-state value is simply referred to as the extensional viscosity, $\eta_E(\dot{\varepsilon}_H)$. Using an EVF, η_E is often unattainable because measurements are limited to Hencky strains of $\varepsilon_H = \ln(L_t/L_0) < 4$, where L_t and L_0 are the specimen length at time t and $t = 0$, respectively. Further deformation is often needed to reach a steady-state value. However, at $\varepsilon_H \gtrsim 4$ the sample rotates back onto itself, which compromises the measurement.[48] Here, $\eta_E(\dot{\varepsilon}_H)$ was attained for too few samples to generate meaningful conclusions.

The linear viscoelastic envelope (LVE) in extension ($\eta_{E,LVE}^+$) was determined from the relationship:

$$\eta_{E,LVE}^+(t) = \lim_{\dot{\varepsilon}_H \to 0} \eta_E^+(t, \dot{\varepsilon}_H) = 3 \lim_{\dot{\gamma} \to 0} \eta^+(t, \dot{\gamma}). \quad (4)$$

Equation 4 is analogous to Trouton's ratio and states that the transient, linear viscoelastic response in extension is a factor of three times larger than that in shear.

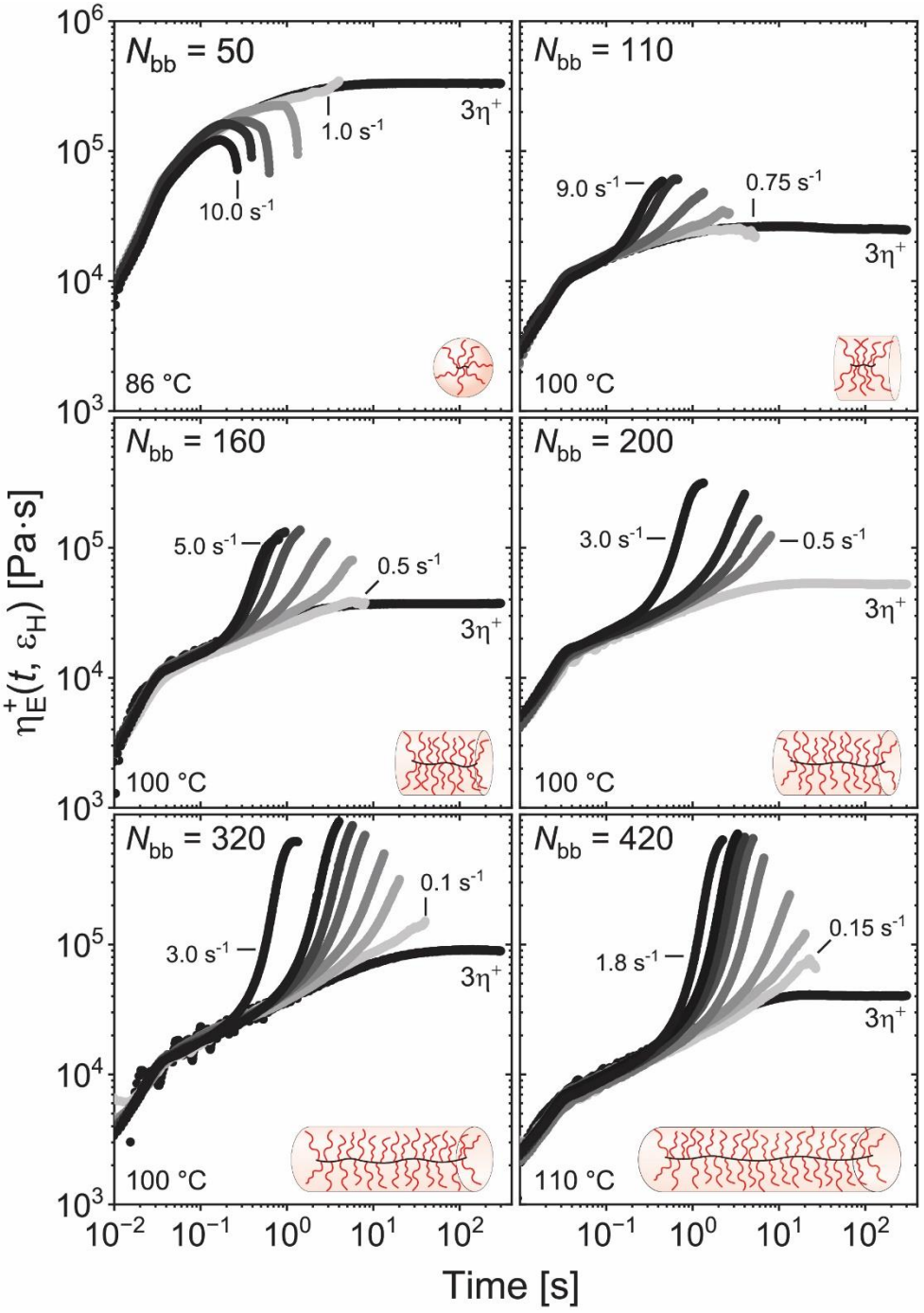

Figure 8. Transient extensional viscosity as a function of time for polymers with $N_{sc} = 72$, taken at various strain rates. The linear viscoelastic envelope is plotted as $3\eta^+$. The Hencky strain rates and temperatures were chosen based on the polymer extensional relaxation time. Strain rates increase from right to left with the limiting bounds shown on the graph. Strain rates for each sample are: $N_{bb} = 50$ [1.0, 3.0, 6.0, 8.0, 10.0 s^{-1}], $N_{bb} = 110$ [0.75, 1.5, 3.0, 6.0, 9.0 s^{-1}], $N_{bb} = 160$ [0.5, 0.7, 1.4, 2.8, 4.3, 5.0 s^{-1}], $N_{bb} = 200$ [0.5, 0.7, 1.0, 3.0 s^{-1}], $N_{bb} = 320$ [0.1, 0.2, 0.3, 0.5, 0.7, 1.0, 3.0 s^{-1}], $N_{bb} = 420$ [0.15, 0.2, 0.3, 0.6, 0.8, 1.0, 1.2, 1.8 s^{-1}].

The transient shear viscosity (η^+) (Figure 8) was measured at a fixed rate ($\dot{\gamma}$) that is within the linear viscoelastic limit (i.e., $\dot{\gamma} \to 0$). Within this limit, the instrument torque at the start of the measurement is small, which can skew the measured value of η^+ (e.g., N_{bb} = 320, Figure 8). For each sample, good agreement between the shear and extensional data was achieved (Figure 8) with quantitative overlap at short times, which provides reassuring validation of the extensional measurements.

MSH, an important processing parameter,[11,12,13,14] refers to the transient non-linear viscoelastic response in extension where η_E^+ increases above $\eta_{E,LVE}^+$ (i.e., $3\eta^+$).[10] All bottlebrush polymers, as identified from the SAOS data, showed evidence of MSH, whereas the star-like polymer (N_{bb} = 50) does not (Figure 8). For the latter, measurements were made at lower temperatures and higher rates to probe shorter relaxation times and ensure no MSH occurs. At temperatures below 86 °C, the melt viscosity is too high to be measured; the sample was pulled out of the rheometer grips during deformation. For the bottlebrush melts, higher temperatures were employed. Deformation rates were chosen according to the relaxation behavior of the materials; as N_{bb} increased, the rate needed to access MSH decreased (Figure 8). Deformation at strain rates larger than those shown here resulted in yielding and melt failure. For the bottlebrush polymers, MSH increases monotonically with N_{bb} (Figure 8). At the fastest rate probed for the largest sample (N_{bb} = 420), η_E^+ increased over an order of magnitude above $3\eta^+$.

The extensional relaxation time (τ_{ext}) that marks the onset of non-linear viscoelastic flow (i.e., MSH) is plotted in Figure 9. This is defined as $\tau_{ext} = 1/\dot{\varepsilon}_c$, where $\dot{\varepsilon}_c$ is the critical Hencky strain rate above which MSH occurs. The value of $\dot{\varepsilon}_c$ can be approximated based on experimental data. Lentzakis et al. approximated $\dot{\varepsilon}_c$ as the slowest Hencky strain rate ($\dot{\varepsilon}_{c,1}$) where MSH is minimized but still observable.[49] The actual value of $\dot{\varepsilon}_c$ is bounded between $\dot{\varepsilon}_{c,1}$ and the fastest Hencky strain rate ($\dot{\varepsilon}_{c,2}$) where linear viscoelastic flow is still maintained. Recognizing that $\dot{\varepsilon}_c$ exists between $\dot{\varepsilon}_{c,1}$ and $\dot{\varepsilon}_{c,2}$, a uniform probability distribution can be used to introduce uncertainty into the determination of $\dot{\varepsilon}_c$ (Figure S9–S13). This improved approach was used to determine

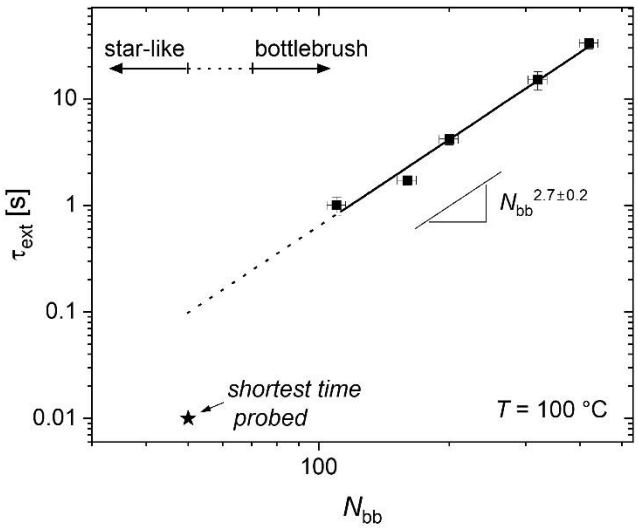

Figure 9. Extensional relaxation time (τ_{ext}), which marks the onset of non-linear viscoelastic flow, plotted as a function of the backbone degree of polymerization (N_{bb}). The backbone degree of polymerization N_{bb} is assumed to have a 5% error. Time-temperature-superposition was used to shift data, where necessary. The solid line is a power law fit ($\tau_{ext} = \left(2.4\times10^{-6}\right) N_{bb}^{2.7\pm0.2}$ [s]) and the dashed line is an extrapolation. The point indicated by a star corresponds to the shortest time probed in extension for the N_{bb} = 50 sample and is not a relaxation time. The star-to-bottlebrush transition identified from SAOS rheometry is indicated on the graph.

$\tau_{ext} \pm \sigma$ for each polymer at T = 100 °C (where σ is a standard deviation), which is plotted in Figure 9 as a function of N_{bb}. With this method, τ_{ext} can only be determined for polymers that exhibit MSH; as a consequence, the result for the N_{bb} = 50 sample is not available. When necessary, data was shifted to T_{ref} = 100 °C using TTS. The relaxation times for the bottlebrush melts follow a power law scaling with N_{bb} (Figure 9), which extrapolates to τ_{ext} = 0.1 s for the star-like polymer (N_{bb} = 50). The shortest time probed in extension for this melt (star, Figure 9) is roughly an order of magnitude smaller, yet no MSH was observed. This suggests that an abrupt scaling transition occurs at the SBT where the relaxation time dramatically shortens for star-like melts.

It is instructive to correlate τ_{ext} to the relaxation spectra collected from SAOS rheology experiments to provide context to its physical meaning. Melts of unentangled linear chains offer a

good point of comparison, since the bottlebrush polymers studied here are also unentangled and follow similar Rouse-like dynamic behavior. For unentangled linear polymers, the relaxation time that marks the onset of melt strain hardening (τ_{ext}) is equal to the longest relaxation time (τ_1), which also happens to be the Rouse time of the entire chain (τ_R).[10,50,51,52] For unentangled bottlebrush melts, no clear crossover between G' and G'' exists marking the onset of terminal flow (Figure 3). Alternatively, the inflection point in $|G^*(\omega)|$ *prior* to terminal flow can be used to identify this transition, which corresponds to the longest relaxation time (τ_1) of the polymer. Figure 10 plots $|G^*(\omega)|$ and its first derivative at $T_{ref} = \bar{T}_g + 34$ °C. The inflection point that indicates τ_1 can be determined from the minimum in the first derivative of $|G^*(\omega)|$ — or when its slope is zero. As shown in Figure 10, the extensional relaxation time associated with the onset of MSH (τ_{ext}) coincides well with the inflection point that marks the onset of terminal flow. This inflection point appears to vanish with decreasing N_{bb}, suggesting that it is correlated with backbone relaxation. As the chains are unentangled, τ_1 likely corresponds to the Rouse time of the entire backbone ($\tau_{R,bb}$), which is the most conformationally restricted part of the chain, so its relaxation time will be the longest. This suggests that τ_{ext} is equivalent to $\tau_{R,bb}$ for unentangled bottlebrush polymers, which underscores the similarity to that of linear unentangled melts. The time $\tau_{R,bb}$ represents the duration needed for an entire bottlebrush chain to diffuse a distance approximately equal to its size. Applying a uniaxial stress at timescales shorter than this (i.e., larger rates) results in non-linear viscoelastic flow via chain orientation and chain stretching, which gives rise to melt strain hardening. Generically, the Rouse time for an unentangled chain is given as:

$$\tau_R \approx \frac{\zeta}{kT} N R_g^{\,2}, \tag{5}$$

where ζ is the friction coefficient, N is the degree of polymerization, R_g is the radius of gyration, and kT is the thermal energy.[53] For an unperturbed Gaussian coil and rigid rod, R_g is proportional to $N^{1/2}$ and N, respectively.[39,53] Accordingly, $\tau_R \sim N^2 \sim M^2$ and $\tau_R \sim N^3 \sim M^3$, respectively. Here, we see that $\tau_{R,bb} \sim N_{bb}^{\,2.7\pm0.2} \sim M_{total}^{\,2.7\pm0.2}$, which lies in between the two

regimes. This is expected since bottlebrush melts are known to form highly extended melt

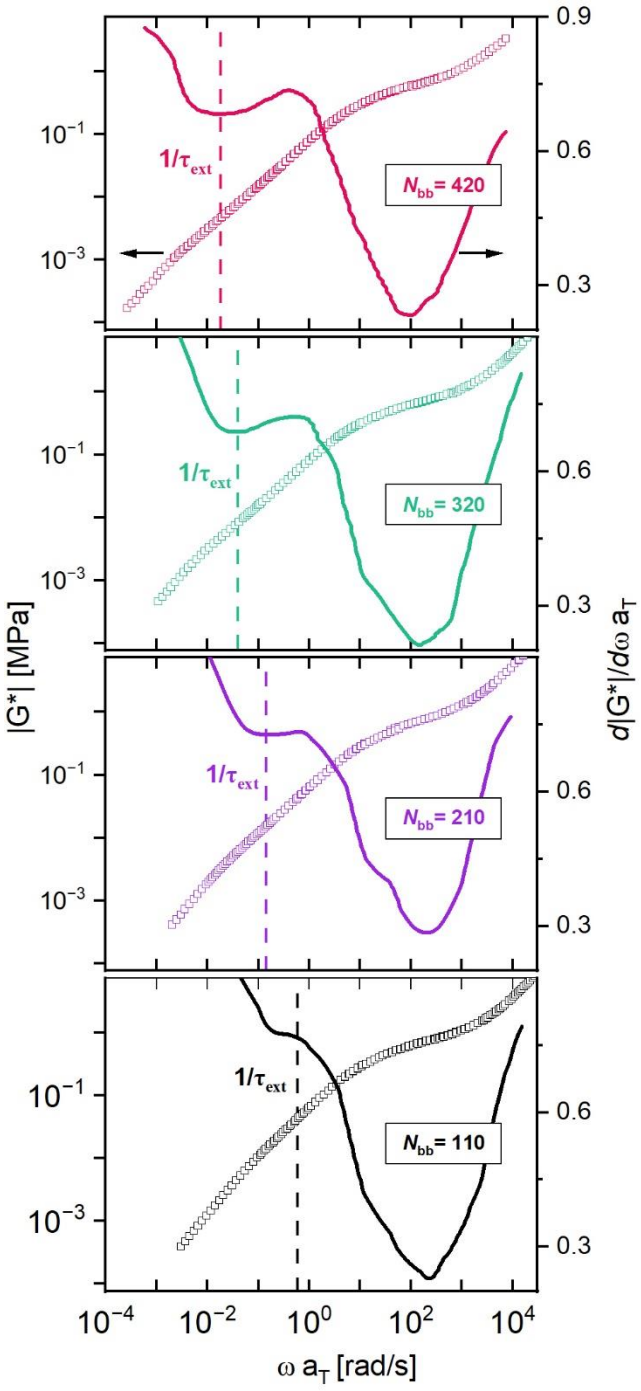

Figure 10. The complex modulus (data points) and its first derivative (solid lines) plotted as a function of frequency using $T_{\text{ref}} = \overline{T}_{\text{g}} + 34$ °C. The dashed line indicates the value of the extensional relaxation time (τ_{ext}) shifted to the same reference temperature and converted to units of rad/s.

conformations, so their behavior should lie somewhere in between that of a coil and rigid rod.

To quantify the extent of MSH, a strain-hardening ratio (SHR) was employed, defined as:

$$\text{SHR} = \eta_E^+(t, \dot{\varepsilon}_H)/\eta_{E,LVE}^+(t) \; . \tag{6}$$

Equation 6 is analogous to Trouton's ratio. When SHR > 1, melt strain hardening is present. The SHR is plotted as a function of $\dot{\varepsilon}_H$ in Figure 11A for each bottlebrush melt with $N_{sc} = 72$. Data

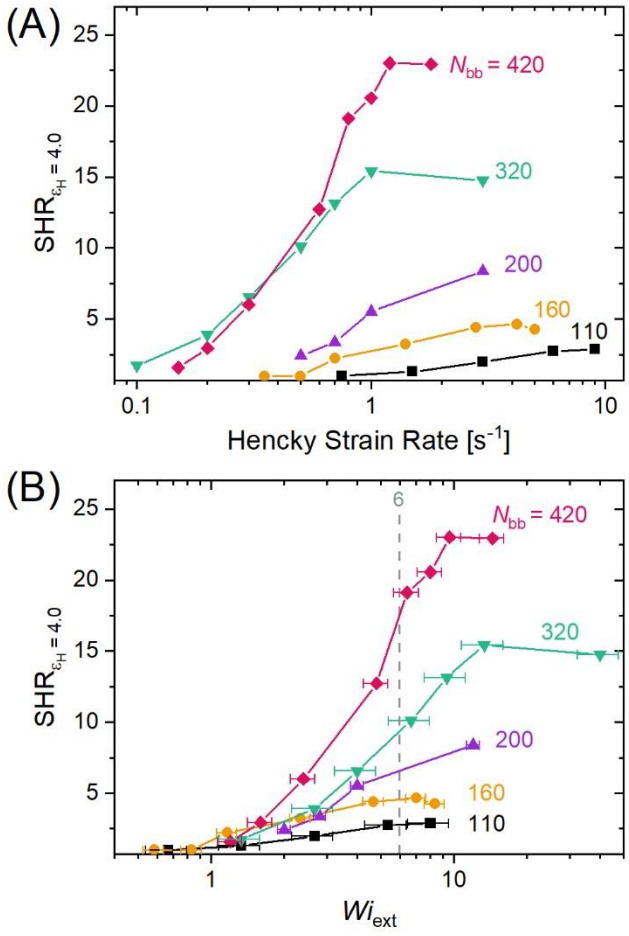

Figure 11. Strain hardening ratio (SHR) for polymers with $N_{sc} = 72$ obtained at a Hencky strain of $\varepsilon_H = 4$ and plotted as a function of (A) the Hencky strain rate ($\dot{\varepsilon}_H$) and (B) the Weissenberg number ($Wi_{ext} = (\tau_{ext} \pm \sigma)\,\dot{\varepsilon}_H$).

were taken at $\varepsilon_H = 4$, the maximum strain measured. In general, increasing N_{bb} results in an increase in the SHR and shifts the data to higher values of $\dot{\varepsilon}_H$. The largest sample ($N_{bb} = 420$) appears to be an exception, due to the data being collected at a slightly higher temperature. To

better compare samples, it is useful to recast $\dot{\varepsilon}_H$ in terms of the Weissenberg number, $Wi_{\text{ext}} = \tau_{\text{ext}}\ \dot{\varepsilon}_H$. This normalizes the data relative to each polymer extensional relaxation time enabling comparisons across different temperatures and architectures. In general, $Wi > 1$ marks the onset of non-linear viscoelastic flow (i.e., MSH). In Figure 11B, the SHR is plotted as a function of Wi_{ext} for each bottlebrush melt. Error bars identify the propagated error associated with τ_{ext}. Strain hardening begins to occur when $Wi_{\text{ext}} \approx 1$, which is expected based on how τ_{ext} was determined. Increasing Wi_{ext} results in an increase in the SHR, which appears to approach a constant value at large Wi_{ext}. When $Wi_{\text{ext}} \gtrsim 2$, differences between samples are apparent, where increasing N_{bb} results in an increase in MSH.

Quantitative comparisons between materials were made by plotting the SHR ($\varepsilon_H = 4$) as a function of N_{bb} for bottlebrush melts with $N_{\text{sc}} = 72$ (Figure 12). The maximum observed SHR

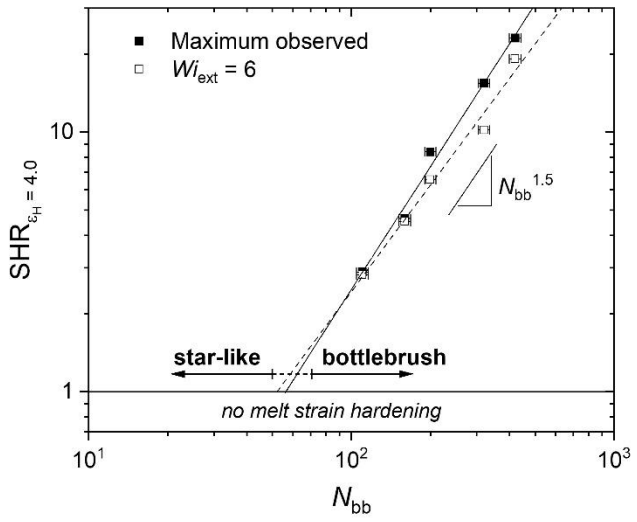

Figure 12. Strain hardening ratio (SHR) for each polymer with $N_{\text{sc}} = 72$ taken at a Hencky strain of $\varepsilon_H = 4$. Data are plotted as a function of the backbone degree of polymerization (N_{bb}), assuming 5% error in N_{bb}. Filled squares correspond to the maximum observed SHR, fitted to a power law function (solid line, SHR ~ $N_{\text{bb}}^{1.6 \pm 0.1}$). Unfilled squares correspond to the SHR at $Wi_{\text{ext}} = \tau_{\text{ext}}\ \dot{\varepsilon}_H = 6$, fitted to a power law function (dashed line, SHR ~ $N_{\text{bb}}^{1.4 \pm 0.1}$). SHR $\leqslant$ 1 designates no melt strain hardening. The star-to-bottlebrush transition identified from SAOS rheometry is indicated on the graph.

(SHR_{max}) is often used as a point of comparison.[16,17] When plotting these data, a power law dependence is evident. This type of behavior is consistent with what has been observed for entangled comb and pom-pom melts, where $SHR \sim M^{1.7}$ and $\sim M^{3}$, respectively.[24] The weaker dependence seen here, $SHR \sim M^{\sim 1.5}$, is possibly due to the lack of chain entanglements or suggestive of a different strain hardening mechanism. This fit can be extrapolated to SHR = 1, which determines the value of N_{bb} that demarcates where MSH is no longer present. This extrapolated value falls within the SBT zone identified from the SAOS data, demonstrating two important points. First, the agreement between extensional and shear behavior emphasizes the fundamental rheological importance of the SBT. Second, the star-like polymers do not appear to melt strain harden in uniaxial extension, which is akin to what has been demonstrated for star polymers with a single branch point.[54,55] The SHR for each polymer was also compared at a constant $Wi_{ext} = 6$ (dashed line, Figure 11B). For $N_{bb} = 160$ and 200, a linear interpolation was used to determine the SHR. These data are plotted in Figure 12, which show good agreement with the SHR_{max} data set, reinforcing the previous conclusions.

Chain stretching is generally accepted as the predominant cause of MSH. [10,50,51] As alluded to earlier, when an unentangled melt is uniaxially deformed at a stretch rate faster than $1/\tau_R$ it will begin to align and stretch in the stress direction, resulting in an entropic restoring force that increases the melt viscosity. Incorporating long chain-branching exacerbates this mechanism by pinning segments of a chain between branch points, which greatly increases the stretch relaxation time.[10] Here, the contribution of chain stretching to the melt viscosity is likely negligible. Firstly, the 'pinned segment' mechanism is non-existent because the side chains are unentangled and the segments between branches are on-average only two repeat units in length. Secondly, each chain is already sterically forced into a stretched conformation prior to deformation, due to the densely packed grafts.[19,20] Entropic loss from additional stretching of the backbone is limited, resulting in a small restoring force,[56] and is one reason why bottlebrush polymers find use as super-soft elastomers.[21,56] Thus, it is unlikely that chain stretching results in the pronounced melt strain

hardening observed here. López-Barrón et al. postulated a different mechanism for MSH in α-olefin bottlebrush polymers: strain-induced intermolecular friction (i.e., frictional drag).[18,27] For

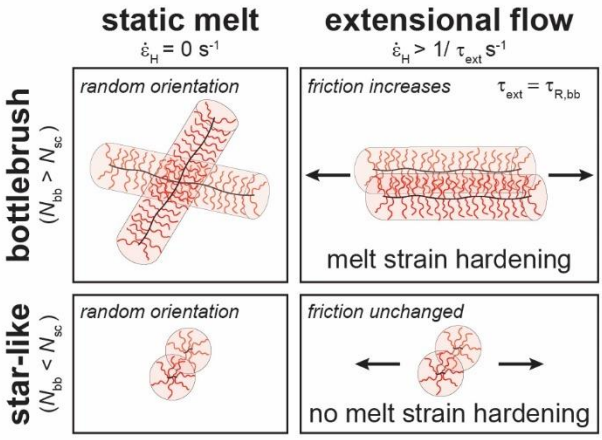

Figure 13. Frictional drag mechanism proposed by López-Barrón et al.,[18] adapted for unentangled bottlebrush melts. In an extensional flow, backbone alignment will occur in the stress direction when the deformation rate ($\dot{\varepsilon}_H$) exceeds the inverse of the Rouse relaxation time of the entire backbone ($\tau_{R,bb}$). This coincides with more side chain interdigitation and frictional drag. For star-like polymers, this mechanism cannot occur due to spherical symmetry, i.e., lack of a preferred molecular orientation.

bottlebrush melts in uniaxial extension, backbone alignment in the flow direction is postulated to force the side-chains to orient towards one another and interdigitate (Figure 13).[18] A sudden *increase* in interdigitation is hypothesized to increase interchain friction, leading to MSH (Figure 13). This mechanism is reliant on backbone orientation in the stress direction so the deformation rate that marks the onset of MSH should coincide with this timescale (Figure 13). Here, we show that this is indeed the case, as each bottlebrush polymer begins to melt strain harden at a stretch rate that coincides with $1/\tau_{R,bb}$ (Figure 10), the rate at which backbone orientation occurs. Further increasing the rate leads to an increase in chain orientation,[27] which explains why MSH increases with $\dot{\varepsilon}_H$ (Figure 11A). We expect frictional drag to be proportional to the number of side chains (q), which justifies the increase of MSH with N_{bb}, since $N_{bb} \sim q$. For star-like polymer melts, this mechanism would not be operative due to the spherical molecular

configurational symmetry; there is no way to orient the chains to promote more side chain interdigitation (Figure 13). Thus, no change in friction upon flow will occur, resulting in no MSH. Here, the transition from star-like to bottlebrush occurs when $N_{bb} > N_{sc}$ (Figure 13). We expect this to be a general trend; however, a more exact description of the transition would depend on the relative length of the side chains (λ_{sc}) to that of the backbone (λ_{bb}), where the bottlebrush limit occurs when $\lambda_{bb} > \lambda_{sc}$.[30]

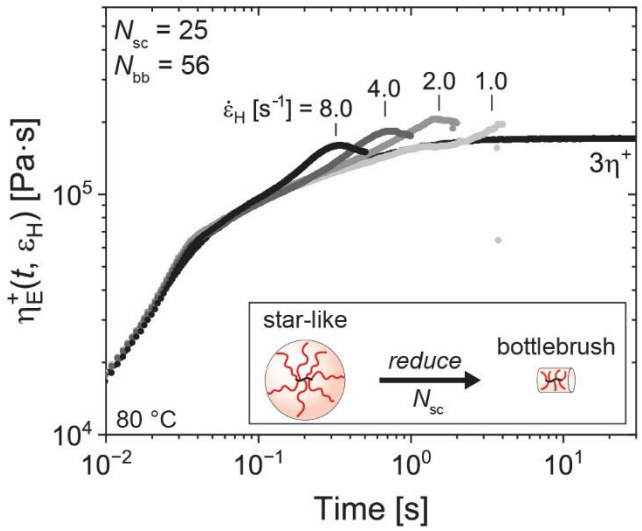

Figure 14. Transient extensional viscosity as a function of time for the polymer with N_{sc} = 25 and N_{bb} = 56. Data were obtained at various Hencky strain rates ($\dot{\varepsilon}_H$). These results, which evidence the onset of MSH, should be compared to the star-like polymer with N_{sc} = 72 and N_{bb} = 50, which does not show MSH. The linear viscoelastic envelope is plotted as $3\eta^+$.

To probe this hypothesis, an additional sample with N_{sc} = 25 and N_{bb} = 56 was synthesized and rheologically compared to the star-like polymer with N_{sc} = 72 and N_{bb} = 50. Based on the proposed mechanism, reducing N_{sc} will induce MSH by shifting the polymer from a spherical, star-like conformation to a more cylindrical conformation. This seems counter-intuitive, as MSH has been shown to decrease with decreasing N_{sc}.[17,49] However, the measurements reveal that weak but discernable MSH is promoted with the reduction in N_{sc} as shown in Figure 14. This result provides clear evidence that side chain interdigitation promotes frictional drag when the backbone is long enough to assume a cylindrical conformation that can align in the direction of applied stress.

Conclusions

A series of model bottlebrush polymers was synthesized using ROMP to probe the star-to-bottlebrush transition in shear and extensional flows. Keeping N_{sc} and z constant, the material functions collected from small-amplitude oscillatory shear measurements were used to establish a star-to-bottlebrush transition as N_{bb} was varied. In the bottlebrush limit, an additional viscoelastic response was recorded at low frequencies, corresponding to backbone relaxation, which is lost when N_{bb} is reduced to the star-limit. In the star-limit, η_0 scales differently with molar mass than conventional star polymers that have branches emanating from a single point. All bottlebrush melts were shown to be unentangled, as evidenced by Rouse-like scaling, $\eta_0 \sim N_{bb}$. We demonstrate that the star-to-bottlebrush transition (SBT) defined in SAOS directly translates to rheological behavior in uniaxial extension.

Extensional viscosity measurements revealed that the bottlebrush polymers melt-strain harden (MSH) whereas the star-like polymers do not. An improved method to experimentally determine the extensional relaxation time (τ_{ext}), which marks the onset of non-linear viscoelasticity, was applied to the materials. We showed that τ_{ext} is equal to the longest relaxation time associated with master curves obtained from SAOS measurements, and that such measurements can be used to estimate the value of the Hencky strain rate $\dot{\varepsilon}_H$ that coincides with MSH in uniaxial extension. Due to the lack of entanglements, τ_{ext} is equivalent to the Rouse time of the backbone ($\tau_{R,bb}$) and follows a scaling dependence with molar mass that is intermediate to that of a Gaussian coil and rigid rod. The onset of MSH in the bottlebrush polymers was explained based on frictional drag as proposed by López-Barrón et al.[18,27] When $\dot{\varepsilon}_H > 1/\tau_{R,bb}$, bottlebrush polymers align in the stress direction causing the side chains to interdigitate, which results in additional chain friction (i.e., drag) and MSH. With star-like polymers there is no molecular orientation due to a spherical molecular configuration, hence no enhanced interdigitation during flow.

This work provides guidelines for improving the processability of bottlebrush melts in strong extensional flows. While the transitions and scaling behavior we show here apply to densely

grafted polymers that are unentangled, we expect the fundamental SBT to be observable for entangled polymers as well. In general, this transition will occur when the chain dimensions shift from a symmetric, spherical conformation to one that is asymmetric and cylindrical. For the polymers studied here, we show that this occurs when $N_{bb} > N_{sc}$. Application to biobased PLA should offer opportunities to enhance the production of materials that rely on strain hardening such as foam and film formation.

Experimental Section

Materials and Graft Polymer Synthesis. The materials and monomers used in this work are described in a previous publication, which also provides a detailed example of the synthesis protocol and describes the methods of molecular characterization.[34] In short, an *exo,exo*-norbornene functionalized poly((±)-lactide) macromonomer was copolymerized with an *endo,exo*-norbornenyl dimethylester comonomer using a Grubbs Generation III catalyst (Figure 1A). Details regarding ^{1}H-NMR and size-exclusion chromatography (SEC) for all monomers can be found in Reference 34. SEC data for each graft polymer is shown in Figures 2 and the associated details regarding molecular characterization of the polymers can be found in Table 1.

Small-Angle X-Ray Scattering (SAXS). SAXS studies were conducted at Sector 5-ID-D of the Advanced Photon Source at Argonne National Laboratories. Samples were hermetically sealed in DSC pans and pre-annealed for 18 hours at 60 °C. 1D-SAXS scattering traces were produced by azimuthally integrating the 2D-SAXS scattering data and calibrated with an Au-coated Si grating with 7200 lines/mm. The 1D patterns plot the magnitude of the scattering wavevector $q = 4\pi \sin(\theta/2)/\lambda$ versus intensity, where θ is the scattering angle and $\lambda = 0.7293$ Å is the radiation wavelength.

Differential Scanning Calorimetry (DSC). DSC measurements were conducted using a Mettler Toledo DSC 1 instrument under a nitrogen gas atmosphere. Samples were loaded into aluminum pans and hermetically sealed. The materials were heated to 150 °C and held isothermally for 12.5

min, then cooled to 25 °C and held isothermally for 5 min. Samples then underwent a second heating ramp to 200 °C. Each thermal ramp rate was 5 °C/min.

Sample Preparation. Films for rheological measurements were made by placing polymer between two Teflon-lined aluminum foil sheets, which were then compression molded using a Wabash Genesis Series Hydraulic Press. Teflon shims were used to achieve a film thickness of 0.6 mm. Materials were processed between 85 and 95 °C, depending on the viscosity of the material. A 500 lbs force was applied for 2.5 min followed by a 1000 lbs force applied for 0.5 min. To avoid water absorption, all samples were stored in a desiccator before and after processing.

Small Amplitude Oscillatory Shear Rheology (SAOS). All rheological measurements were obtained using an ARES-G2 Rheometer (TA Instruments). SAOS measurements were performed using an 8.0 mm parallel plate geometry with a gap of ~0.5 mm. Instrument compliance effects are assumed to be negligible due to the relatively small moduli of each material at the frequencies probed. Frequency sweeps were gathered at temperatures between 57 °C < T < 150 °C, depending on the polymer. Frequencies between 0.1 rad/s < ω < 100 rad/s were applied using a strain amplitude between 0.1% < γ < 10%. The strain amplitude was chosen based on results from strain amplitude sweeps at different temperatures and strain rates. Values were chosen within the limit of linear viscoelasticity. Master curves were created for each material by shifting the data to $T_{ref} = \overline{T}_g + 34$ °C using time-temperature superposition (TTS). Trios software was used to apply TTS and to differentiate material functions.

Steady Shear Rheology. Experiments were conducted using a 8.0 mm cone and plate geometry with a truncation gap of 0.0528 mm. The measurements were obtained at temperatures of 80 to 110 °C and shear rates of $\dot{\gamma} = 0.01$ to 0.1 s^{-1}. Multiple experiments were performed at these low shear rates to ensure linear viscoelastic behavior. In some cases, minor evidence of shear thinning was observed. For these samples, the extent of thinning was small and occurred at times greater than those associated with the extensional measurements, which means it does not influence any calculations associated with the strain hardening ratios.

Uniaxial Extensional Rheology. Measurements were performed on 10 mm x 15 mm x 0.6 mm rectangular samples using an Extensional Viscosity Fixture (EVF). The measurements were performed at temperatures of 80 to 110 °C and Hencky strain rates $\dot{\varepsilon}_H \leq 10$ s^{-1}, i.e., up to the maximum rate that can be applied. Samples were deformed to a Hencky strain of $\varepsilon_H = 4$, which is roughly the maximum strain possible without wrapping the sample back onto itself. To mitigate sagging, measurements were initiated quickly after loading samples on the EVF. In some cases, a pre-stretching procedure was performed to account for sag where the sample was extended to a small strain at a rate chosen such that $\dot{\varepsilon}_H \ll 1/\tau_{ext}$.

Supporting Information

Small-angle x-ray scattering, differential scanning calorimetry, supplemental small-amplitude oscillatory shear data, supplemental extensional data, discussion of two-regime model.

Author Information

Corresponding Authors:

Marc A. Hillmyer – Department of Chemistry, University of Minnesota, Minneapolis, MN, 55455-0431, United States; orcid.org/0000-0001-8255-3853; Email: hillmyer@umn.edu

Frank S. Bates – Department of Chemical Engineering and Materials Science, University of Minnesota, Minneapolis, MN, 55455-0132, United States; orcid.org/0000-0003-3977-1278; Email: bates001@umn.edu

Co-Authors:

Aristotelis Zografos – Department of Chemical Engineering and Materials Science, University of Minnesota, Minneapolis, MN, 55455-0132, United States; orcid.org/0000-0001-9612-091X

Helena A. All – Department of Chemistry, University of Minnesota, Minneapolis, MN, 55455-0431, United States

Alice B. Chang – Department of Chemical Engineering and Materials Science, University of Minnesota, Minneapolis, MN, 55455-0132, United States; orcid.org/0000-0001-5036-2681

Notes:

The authors declare no competing financial interest.

Acknowledgements

We thank the National Science Foundation (NSF) Center for Sustainable Polymers (CHE-1901635) at the University of Minnesota, as well as the NSF Graduate Research Fellowship Program (DGE-1839286) for financial support. ^{1}H-NMR experiments were conducted at the University of Minnesota Nuclear Magnetic Resonance Laboratory using an instrument that is supported by the Director, National Institutes of Health (S10OD011952). The content of this work is solely the responsibility of the authors and does not necessarily represent the official views of the National Institutes of Health. Portions of this work were performed at the DuPont-Northwestern-Dow Collaborative Access Team (DND-CAT) located at Sector 5 of the Advanced Photon Source (APS). DND-CAT is supported by Northwestern University, The Dow Chemical Company, and DuPont de Nemours, Inc. This research used resources of the Advanced Photon Source, a U.S. Department of Energy (DOE) Office of Science User Facility operated for the DOE Office of Science by Argonne National Laboratory under Contract No. DE-AC02-06CH11357. We thank Zachary Gdowski, Joanna White, and Camila Perales-Rodriguez for their help in the collection of the SAXS data. We thank Prof. Chris W. Macosko and Prof. Michelle A. Calabrese for helpful discussions regarding rheology. We thank Dr. David Giles for helpful guidance regarding melt processing, SAOS rheological measurements, and extensional rheological measurements. We thank Erin M. Maines, Michael B. Sims, Diana Y. Zhang, Patrick McCauley and Daniel Krajovic for helpful discussions and feedback related to the work. We also acknowledge Dr. Christopher DeRosa for providing the *exo,exo*-norbornene alcohol initiator used to synthesize the macromonomers. We also thank James Bamford for early contributions regarding the extensional rheology of graft block polymers.

References

[1] Haque, F. M.; Ishibashi, J. S. A.; Lidston, C. A. L.; Shao, H.; Bates, F. S.; Chang, A. B.; Coates, G. W.; Cramer, C. J.; Dauenhauer, P. J.; Dichtel, W. R.; Ellison, C. J.; Gormong, E. A.; Hamachi, L. S.; Hoye, T. R.; Jin, M.; Kalow, J. A.; Kim, H. J.; Kumar, G.; LaSalle, C. J.; Liffland, S.; Lipinski, B. M.; Pang, Y.; Parveen, R.; Peng, X.; Popowski, Y.; Prebihalo, E. A.; Reddi, Y.; Reineke, T. M.; Sheppard, D. T.; Swartz, J. L.; Tolman, W. B.; Vlaisavljevich, B.; Wissinger, J.; Xu, S.; Hillmyer, M. A. Defining the Macromolecules of Tomorrow through Synergistic Sustainable Polymer Research. *Chem. Rev.* **2022**, *122*, 6322–6373.

[2] European Bioplastics, Bioplastics Market Data. https://www.european-bioplastics.org/market/ (accessed 2022-11-5)

[3] Lim, L.-T.; Auras, R.; Rubino, M. Processing Technologies for Poly(Lactic Acid). *Prog. Polym. Sci.* **2008**, *33*, 820–852.

[4] Nofar, M.; Park, C. B. Poly (Lactic Acid) Foaming. *Prog. Polym. Sci.* **2014**, *39*, 1721–1741.

[5] Nofar, M.; Park, C. B. Introduction to Polylactide and Polylactide Foaming. In *Polylactide Foams*; Elsevier, **2018**, 17–34.

[6] Tadmor, Z.; Gogos, C. G. *Principles of Polymer Processing, Second Edition*; Wiley-Interscience, **2006**.

[7] Yahyaee, N.; Javadi, A.; Garmabi, H.; Khaki, A. Effect of Two-Step Chain Extension Using Joncryl and PMDA on the Rheological Properties of Poly (Lactic Acid). *Macromol. Mater. Eng.* **2020**, *305* (2), 1900423.

[8] Mallet, B.; Lamnawar, K.; Maazouz, A. Improvement of Blown Film Extrusion of Poly(Lactic Acid): Structure-Processing-Properties Relationships. *Polym. Eng. Sci.* **2014**, *54* (4), 840–857.

[9] Gu, L.; Xu, Y.; Fahnhorst, G. W.; Macosko, C. W. Star vs Long Chain Branching of Poly(Lactic Acid) with Multifunctional Aziridine. *J. Rheol.* **2017**, *61*, 785–796.

[10] Dealy, J. M.; Read, D. J.; Larson, R. G. *Structure and Rheology of Molten Polymers: From Structure to Flow Behavior and Back Again*; Hanser Publishers, **2018**.

[11] Münstedt, H. Extensional Rheology and Processing of Polymeric Materials. *Int. Polym. Process.* **2018**, *33*, 594–618.

[12] Münstedt, H.; Steffl, T.; Malmberg, A. Correlation between Rheological Behaviour in Uniaxial Elongation and Film Blowing Properties of Various Polyethylenes. *Rheol. Acta* **2005**, *45*, 14–22.

[13] Münstedt, H.; Kurzbeck, S.; Stange, J. Importance of Elongational Properties of Polymer Melts for Film Blowing and Thermoforming. *Polym. Eng. Sci.* **2006**, *46*, 1190–1195.

[14] Spitael, P.; Macosko, C. W. Strain Hardening in Polypropylenes and Its Role in Extrusion Foaming. *Polym. Eng. Sci.* **2004**, *44*, 2090–2100.

[15] McLeish, T. C. B.; Larson, R. G. Molecular Constitutive Equations for a Class of Branched Polymers: The Pom-Pom Polymer. *J. Rheol.* **1998**, *42*, 81–110.

[16] Abbasi, M.; Faust, L.; Riazi, K.; Wilhelm, M. Linear and Extensional Rheology of Model Branched Polystyrenes: From Loosely Grafted Combs to Bottlebrushes. *Macromolecules* **2017**, *50*, 5964–5977.

[17] López-Barrón, C. R.; Shivokhin, M. E.; Hagadorn, J. R. Extensional Rheology of Highly-Entangled α-Olefin Molecular Bottlebrushes. *J. Rheol.* **2019**, *63*, 917–926.

[18] López-Barrón, C. R.; Shivokhin, M. E. Extensional Strain Hardening in Highly Entangled Molecular Bottlebrushes. *Phys. Rev. Lett.* **2019**, *122*, 037801.

[19] Paturej, J.; Sheiko, S. S.; Panyukov, S.; Rubinstein, M. Molecular Structure of Bottlebrush Polymers in Melts. *Sci. Adv.* **2016**, *2*, e1601478.

[20] Liang, H.; Cao, Z.; Wang, Z.; Sheiko, S. S.; Dobrynin, A. V. Combs and Bottlebrushes in a Melt. *Macromolecules* **2017**, *50*, 3430–3437.

[21] Daniel, W. F. M.; Burdyńska, J.; Vatankhah-Varnoosfaderani, M.; Matyjaszewski, K.; Paturej, J.; Rubinstein, M.; Dobrynin, A. V.; Sheiko, S. S. Solvent-Free, Supersoft and Superelastic Bottlebrush Melts and Networks. *Nat. Mater.* **2016**, *15*, 183–189.

[22] Liang, H.; Morgan, B. J.; Xie, G.; Martinez, M. R.; Zhulina, E. B.; Matyjaszewski, K.; Sheiko, S. S.; Dobrynin, A. V. Universality of the Entanglement Plateau Modulus of Comb and Bottlebrush Polymer Melts. *Macromolecules* **2018**, *51*, 10028–10039.

[23] Haugan, I. N.; Maher, M. J.; Chang, A. B.; Lin, T.; Grubbs, R. H.; Hillmyer, M. A.; Bates, F. S. Consequences of Grafting Density on the Linear Viscoelastic Behavior of Graft Polymers. *ACS Macro Lett.* **2018**, *7*, 525–530.

[24] Abbasi, M.; Faust, L.; Wilhelm, M. Comb and Bottlebrush Polymers with Superior Rheological and Mechanical Properties. *Adv. Mater.* **2019**, *31*, 1806484.

[25] Wingstrand, S. L.; Alvarez, N. J.; Huang, Q.; Hassager, O. Linear and Nonlinear Universality in the Rheology of Polymer Melts and Solutions. *Phys. Rev. Lett.* **2015**, *115*, 078302.

[26] O'Connor, T. C.; Alvarez, N. J.; Robbins, M. O. Relating Chain Conformations to Extensional Stress in Entangled Polymer Melts. *Phys. Rev. Lett.* **2018**, *121*, 047801.

[27] López-Barrón, C. R.; Burghardt, W. R.; Kweon, M. S. Local and Global Stretching of Polymer Chains during Startup of Extensional Flow. *ACS Macro Lett.* **2020**, *9*, 26–31.

[28] Dalsin, S. J.; Hillmyer, M. A.; Bates, F. S. Molecular Weight Dependence of Zero-Shear Viscosity in Atactic Polypropylene Bottlebrush Polymers. *ACS Macro Lett.* **2014**, *3*, 423–427.

[29] Dalsin, S. J.; Hillmyer, M. A.; Bates, F. S. Linear Rheology of Polyolefin-Based Bottlebrush Polymers. *Macromolecules* **2015**, *48*, 4680–4691.

[30] Levi, A. E.; Lequieu, J.; Horne, J. D.; Bates, M. W.; Ren, J. M.; Delaney, K. T.; Fredrickson, G. H.; Bates, C. M. Miktoarm Stars via Grafting-Through Copolymerization: Self-Assembly and the Star-to-Bottlebrush Transition. *Macromolecules* **2019**, *52*, 1794–1802.

[31] Pesek, S. L.; Li, X.; Hammouda, B.; Hong, K.; Verduzco, R. Small-Angle Neutron Scattering Analysis of Bottlebrush Polymers Prepared via Grafting-Through Polymerization. *Macromolecules* **2013**, *46*, 6998–7005.

[32] Lin, T.-P.; Chang, A. B.; Chen, H.-Y.; Liberman-Martin, A. L.; Bates, C. M.; Voegtle, M. J.; Bauer, C. A.; Grubbs, R. H. Control of Grafting Density and Distribution in Graft Polymers by Living Ring-Opening Metathesis Copolymerization. *J. Am. Chem. Soc.* **2017**, *139*, 3896–3903.

[33] Chang, A. B.; Lin, T.-P.; Thompson, N. B.; Luo, S.-X.; Liberman-Martin, A. L.; Chen, H.-Y.; Lee, B.; Grubbs, R. H. Design, Synthesis, and Self-Assembly of Polymers with Tailored Graft Distributions. *J. Am. Chem. Soc.* **2017**, *139*, 17683–17693.

[34] Zografos, A.; Lynd, N. A.; Bates, F. S.; Hillmyer, M. A. Impact of Macromonomer Molar Mass and Feed Composition on Branch Distributions in Model Graft Copolymerizations. *ACS Macro Lett.* **2021**, *10*, 1622–1628.

[35] Radzinski, S. C.; Foster, J. C.; Chapleski, R. C.; Troya, D.; Matson, J. B. Bottlebrush Polymer Synthesis by Ring-Opening Metathesis Polymerization: The Significance of the Anchor Group. *J. Am. Chem. Soc.* **2016**, *138*, 6998–7004.

[36] López-Barrón, C. R.; Brant, P.; Eberle, A. P. R.; Crowther, D. J. Linear Rheology and Structure of Molecular Bottlebrushes with Short Side Chains. *J. Rheol.* **2015**, *59*, 865–883.

[37] Tsukahara, Y.; Namba, S.; Iwasa, J.; Nakano, Y.; Kaeriyama, K.; Takahashi, M. Bulk Properties of Poly(Macromonomer)s of Increased Backbone and Branch Lengths. *Macromolecules* **2001**, *34*, 2624–2629.

[38] Hu, M.; Xia, Y.; McKenna, G. B.; Kornfield, J. A.; Grubbs, R. H. Linear Rheological Response of a Series of Densely Branched Brush Polymers. *Macromolecules* **2011**, *44*, 6935–6943.

[39]Lodge, T. P.; Hiemenz, P. C. *Polymer Chemistry*; Taylor and Francis Group, **2007**.

[40] van Gurp, M.; Palmen, J. Time-Temperature Superposition for Polymeric Blends. *J. Rheol. Bull.* **1998**, *67*, 5–8.

[41] Qian, Z.; McKenna, G. B. Expanding the Application of the van Gurp-Palmen Plot: New Insights into Polymer Melt Rheology. *Polymer* **2018**, *155*, 208–217.

[42] Kempf, M.; Ahirwal, D.; Cziep, M.; Wilhelm, M. Synthesis and Linear and Nonlinear Melt Rheology of Well-Defined Comb Architectures of PS and PpMS with a Low and Controlled Degree of Long-Chain Branching. *Macromolecules* **2013**, *46*, 4978–4994.

[43] Zimm, B. H. Dynamics of Polymer Molecules in Dilute Solution: Viscoelasticity, Flow Birefringence and Dielectric Loss. *J. Chem. Phys.* **1956**, *24*, 269–278.

[44] Fetters, L. J.; Kiss, A. D.; Pearson, D. S.; Quack, G. F.; Vitus, F. J. Rheological Behavior of Star-Shaped Polymers. *Macromolecules* **1993**, *26*, 647–654.

[45] Milner, S. T.; McLeish, T. C. B. Parameter-Free Theory for Stress Relaxation in Star Polymer Melts. *Macromolecules* **1997**, *30*, 2159–2166.

[46] Milner, S. T.; McLeish, T. C. B. Arm-Length Dependence of Stress Relaxation in Star Polymer Melts. *Macromolecules* **1998**, *31*, 7479–7482.

[47] Vega, D. A.; Sebastian, J. M.; Russel, W. B.; Register, R. A. Viscoelastic Properties of Entangled Star Polymer Melts: Comparison of Theory and Experiment. *Macromolecules* **2002**, *35*, 169–177.

[48] TA Instruments PN002. *The ARES-EVF: Option for Measuring Extensional Viscosity of Polymer Melts*. TA Instruments. https://www.tainstruments.com/pdf/literature/APN002_V2_ARES_EVF_to_measure_elongation_viscosity.pdf (accessed 2022-11-04).

[49] Lentzakis, H.; Vlassopoulos, D.; Read, D. J.; Lee, H.; Chang, T.; Driva, P.; Hadjichristidis, N. Uniaxial Extensional Rheology of Well-Characterized Comb Polymers. *J. Rheol.* **2013**, *57*, 605–625.

[50] Ianniruberto, G.; Marrucci, G.; Masubuchi, Y. Melts of Linear Polymers in Fast Flows. *Macromolecules* **2020**, *53*, 5023–5033

[51] Huang, Q. When Polymer Chains Are Highly Aligned: A Perspective on Extensional Rheology. *Macromolecules* **2022**, *55*, 715–727

[52] Watanabe, H.; Matsumiya, Y. Nonlinear Elongational Rheology of Unentangled Polystyrene and Poly(*p*-*tert*-butylstyrene) Melts. *Macromolecules* **2018**, *51*, 9710-9729.

[53] Rubenstein, M.; Colby, R. H. *Polymer Physics*; Oxford University Press, 2003.

[54] Ianniruberto, G.; Marrucci, G. Entangled Melts of Branched PS Behave Like Linear PS in the Steady State of Fast Elongational Flows. *Macromolecules* **2013**, *46*, 267–275.

[55] Huang, Q.; Agostini, S.; Hengeller, L.; Shivokhin, M.; Alvarez, N. J.; Hutchings, L. R.; Hassager, O. Dynamics of Star Polymers in Fast Extensional Flow and Stress Relaxation. *Macromolecules* **2016**, *49*, 6694–6699.

[56] Zhulina, E. B.; Sheiko, S. S.; Borisov, O. V. Solution and Melts of Barbwire Bottlebrushes: Hierarchical Structure and Scale-Dependent Elasticity. *Macromolecules* **2019**, *52*, 1671–1684.